Current Applied Physics 11 (2011) 1410–1413

Contents lists available at ScienceDirect

Current Applied Physics

journal homepage: www.elsevier.com/locate/cap

High efficiency top-emitting white organic light-emitting devices with a (metal/organic)$_2$ cathode

Wenyu Ji [a,b,c], Letian Zhang [a,*], Mo Liu [a], Jing Wang [b], Guoqiang Liu [b], Wenfa Xie [a,*], Hanzhuang Zhang [b]

[a] State Key Laboratory on Integrated Optoelectronics, College of Electronic Science and Engineering, Jilin University, Qianjin Street 2699, Changchun 130012, China
[b] Department of Physics, Jilin University, Changchun 130023, China
[c] Key Laboratory of Excited State Processes, Changchun Institute of Optics, Fine Mechanics and Physics, Chinese Academy of Sciences, Changchun 130033, People's Republic of China

ARTICLE INFO

Article history:
Received 7 November 2010
Received in revised form
13 April 2011
Accepted 14 April 2011
Available online 30 April 2011

Keywords:
White OLED
Top-emitting
Metal/organic multilayer

ABSTRACT

White top-emitting organic light-emitting devices (TEOLEDs) were fabricated on a glass substrate with metal/organic multilayer of $(Ag/Alq_3)_2$ (Alq_3 is tris-(8-hydroxyquinoline) aluminum) as cathode. White TEOLEDs with high efficiency were obtained due to the microcavity effects. And the $(Ag/Alq_3)_2$ cathode, which adjusted the optical characteristics of the devices, played an important role. In addition, Alq_3–Ag–Alq_3 multilayer could work as a buffer layer, which would simplify the process of encapsulation for devices. We also calculated the electroluminescence spectrum of devices encapsulated with Al_2O_3 (150 nm) and Al_2O_3(75 nm)/ZrO_2(75 nm). And the results indicated that the CIE coordinates is almost the same between with and without encapsulating.

1. Introduction

White organic light-emitting devices (WOLEDs) have aroused a great deal of attention in the past decade because of their potential use in full-color flat-panel displays and lighting source. In particular, top-emitting organic light-emitting devices (TEOLEDs) have much more advantages than the bottom-emitting one in flat-panel displays due to higher aperture ratio. Thus, white TEOLEDs are particularly suitable for high-resolution active matrix displays and solid state lighting. In addition, one of the advantages of OLEDs, compared with other display technologies, is the possibility of making flexible displays [1–4]. In order to apply, encapsulation is important for OLED to prevent light-emitting materials and electrodes by blocking permeation of water vapor and ambient oxygen, and to protect devices from external shocks. Thin-film encapsulation is indispensible to realize top-emission OLED (TEOLED) without desiccant [5]. In addition, the CIE color coordinates should not change when the devices are encapsulated. Previously, a number of different schemes for thin-film encapsulation were reported in the literature [3,6–8]. Recently, Al_2O_3 and hybrid multilayers with polyurea/Al_2O_3 and Al_2O_3/ZrO_2 were used in thin-film encapsulation [9,10].

However, it remains a challenge to generate white light in TEOLEDs because of the strong microcavity effects in the devices. Thus, extensive efforts have focused on eliminating the microcavity effects in white TEOLEDs [11–14]. Besides, Kim et al reported the TEWOLED utilizing microcavity effects [15], M. Thomschke et al reported the TEWOLED with optimized efficiency and angular emission characteristics [16], and TEWOLED with down-conversion phosphors was reported by Ji et al. [17]. A three-peak bottom-emitting white organic light-emitting devices with thin metal/dielectric/thin metal/dielectric/thick metal as cathode was reported by Lu et al. [18]. In addition, a three-peak or two-peak TEWOLED with metallic-dielectric photonic crystal anode were reported in our previous work [19,20]. However, all the reported TEWOLEDs will have some issues when building flexible OLEDs, for which thin-film encapsulation is necessary. For all the devices reported above, a buffer layer must be deposited on the top cathode for encapsulating. And this may change the optical characteristic of the devices, for example, the spectrum and the CIE coordinates. In this paper, we report the white TEOLEDs utilizing microcavity effects with multi-layer [Ag/tris-(8-hydroxyquinoline) aluminum]$_2$ as cathode (tris-(8-hydroxyquinoline) aluminum is Alq_3), which can be encapsulated directly.

It is well known that the resonance wavelength (RW) of a cavity is a dominant factor in the determination of the emission wavelength of a device using a microcavity structure. According to the resonant conditions of the microcavity, the RW of a microcavity for normal incidence is determined by the Fabry–Perot peak condition [21]:

$$\sum_i \frac{4\pi d_i n_i(\lambda)}{\lambda} - \varphi_{\text{cathode}}(0,\lambda) - \varphi_{\text{anode}}(0,\lambda) = 2m\pi$$

* Corresponding authors.
E-mail addresses: zlt@jlu.edu.cn (L. Zhang), xiewf@jlu.edu.cn (W. Xie).

1567-1739/$ – see front matter © 2011 Elsevier B.V. All rights reserved.
doi:10.1016/j.cap.2011.04.013

where λ is the emission wavelength, $\varphi_{cathode}(0,\lambda)$ and $\varphi_{anode}(0,\lambda)$are the angle- and the wavelength-dependent phase changes on reflection from the top cathode and the bottom anode, respectively, and m is an integer that defines the mode number, $n_i(\lambda)$ and d_i are the refractive index and the thickness of the organic layers. Based on such a principle, to achieve a multiple-peak WOLED showing EL peaks at desired wavelengths, one shall modify the phase property to satisfy the Fabry–Perot peak condition at desired wavelengths. Such cathode could be realized by multilayers of stacking organic materials and thin metal layer. In order to obtain strong microcavity effect, we chose Ag as anode due to its high reflectance over the whole visible range.

2. Experimental

The top-emitting devices with a structure of silica coated silicon substrate/Ag (150 nm)/MoO_x (1.5 nm)/4,4′,4″-tris(3-methylphenyl-phenylamino)-tripheny-lamine (m-MTDATA, 30 nm)/N,N′-bis-(1-naphthyl)-N,N'diphenyl-1,1-biphenyl-4,4'diamine (NPB, 10 m)/4,4′-bis(2,2′-diphenylvinyl)-1,1′-biphenyl (DPVBi, 15 nm)/4,4-*N*,*N*-dicarbazole-biphenyl (CBP, 3 nm)/CBP:bis(2-(2-fluorphenyl)-1,3-benzothiozolato- N,C2′) iridium(acetylacetonate) [$(F\text{-}BT)_2Ir(acac)$] (7 nm)/4,7-diphenyl −1,10-phenanthroline (Bphen, 35 nm)/LiF (1 nm)/Al (1 nm)/[Ag(20 nm)/Alq_3(x nm)]$_2$ were fabricated. In the devices, Ag/MoO_x, m-MTDATA, NPB, DPVBi, CBP: $(F\text{-}BT)_2Ir(acac)$, Bphen, and LiF/Al/$(Ag/Alq_3)_2$ were used as anode, hole injection layer, hole transporting layer, blue emitting layer, orange emitting layer, electron transporting layer and cathode, respectively. x = 75 and 85 for cathode 1 (devices A) and cathode 2 (devices B), respectively. The neat CBP is introduced to separate blue and orange emitting layers. For comparison, the bottom-emitting device (ITO glass substrate) with the same organic layers (device C) was fabricated, which have the structure of ITO-coated glass substrate/m-MTDATA(30 nm)/NPB(10 nm)/DPVBi(15 nm)/CBP(3 nm)/CBP:[$(F\text{-}BT)_2Ir(acac)$] (7 nm)/Bphen(35 nm)/LiF (1 nm)/Al (200 nm). All films were deposited at pressure below 4×10^{-6} Torr. The deposition of each layer and the measure of devices characteristics were described before [17].

3. Results and discussion

Fig. 1(a) shows the calculated round-trip phase changes for 100 nm organic layers sandwiched between two reflection electrodes [i.e., $\varphi_1(\lambda) = \sum 4\pi d_i n_i(\lambda)/\lambda$], and the phase changes at two reflective electrodes for normal incidence [i.e., $\varphi_2(0,\lambda) = \varphi_{cathode}(0,\lambda) + \varphi_{anode}(0,\lambda)$, incidence medium is Bphen and m-MTDATA for cathode and anode, respectively]. The points of the intersection of $\varphi_1(\lambda)$ and $\varphi_2(\lambda)$ are the RWs of the devices. Alq_3 is used as the dielectric material not only due to its stability and low cost, but also due to its high transparency in the visible range and compatibility with the OLED fabrication [22]. Ag is used as the metal due to its lower absorption loss in the visible range and highest conductivity among electrode materials. The phase shift is calculated by the transfer-matrix method [23]. As can be seen, two RWs peaks were obtained for device A (447 nm and 559 nm) and device B (460 nm and 569 nm). Fig. 1(b) shows the reflectance and transmittance of the two cathodes. Moderate reflectance is obtained at RWs, which insures strong microcavity effects in the devices. As can be seen, at short wavelength the reflectance of cathode 2 is higher than that of cathode 1, so we can estimate that the blue emission will be stronger in device B than that of device A.

Fig. 2(a) shows the normalized measured EL spectra at voltage of 6, 8, and 10 V for device A. The spectrum of the device A shows two peaks at 452 and 560 nm due to microcavity effects. Insert is the normalized measured EL spectra at voltage of 6 V for viewing angle of 0°, 30°, and 60°. As can be seen, with increasing viewing angle,

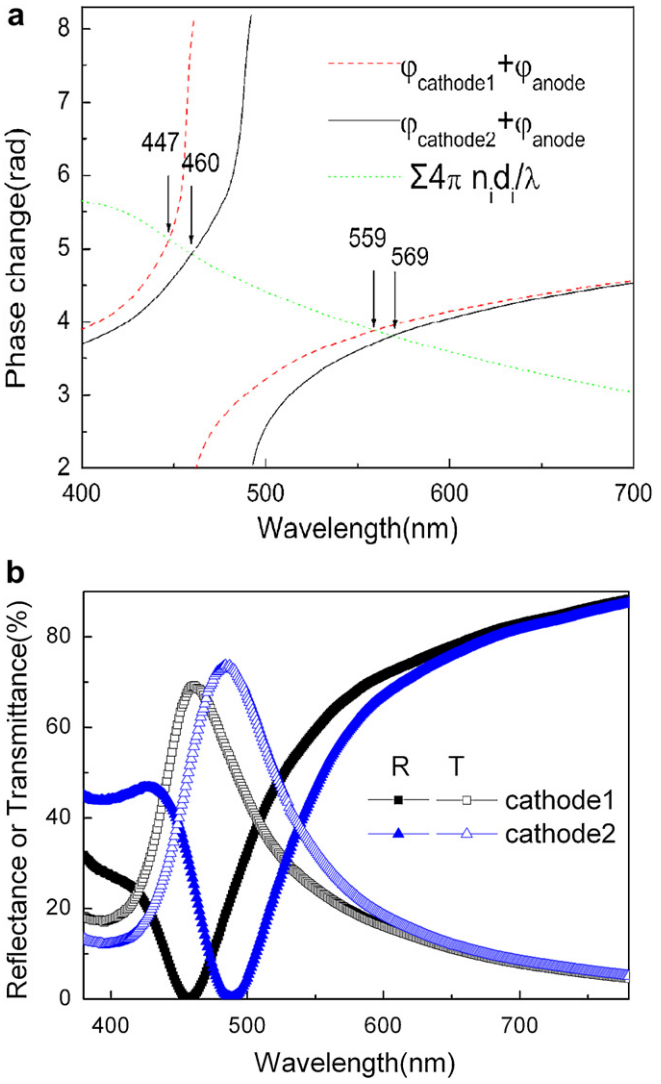

Fig. 1. (a). The calculated round-trip phase changes for 100 nm organic layers between two electrodes [i.e., $\varphi_1(\lambda) = \sum 4\pi d_i n_i(\lambda)/\lambda$] and the phase changes for two electrodes [i.e., $\varphi_2(0,\lambda) = \varphi_{cathode}(0,\lambda) + \varphi_{anode}(0,\lambda)$]; (b) The reflectance and transmittance of the cathodes.

the peak wavelength shifts to a shorter wavelength due to the microcavity effects in the TEOLEDs. A warm white emission was obtained, and the Commission Internationale de l'Eclairage (CIE) coordinates (at voltage of 6 V) were (0.308, 0.376) at a viewing angle of 0° and changed to (0.288, 0.406) at 30° and (0.245 0.390) at 60°. Fig. 2(b) shows the normalized measured EL spectra at voltage of 6, 8, and 10 V for device B. The spectrum of the device B also shows two peaks at 464 and 568 nm due to microcavity effects. And red shift of the resonant peaks was observed relative to device A. All the results was due to the utilizing of thicker Alq_3 layer,85 nm Alq_3 for device B. Insert is the normalized measured EL spectra at voltage of 6, 8, and 10 V for device C, which shows two main peaks at 448 and 548 nm originating from DPVBi and $(F\text{-}BT)_2Ir(acac)$. In devices A and B, the resonant peaks are near the DPVBi and $(F\text{-}BT)_2Ir(acac)$ emission peaks which results in the comparable efficiency to the device C. Comparing Fig. 2(a) with Fig. 2(b),we find that the blue emission intensity relative to the orange emission is stronger for device B than that of device A. And this result is in excellent agreement with our estimation. Fig. 2(c) shows the normalized measured EL spectra at different viewing angle of 0°, 30°, and 60° and a voltage of 6 V for device B. The spectrum of the device B

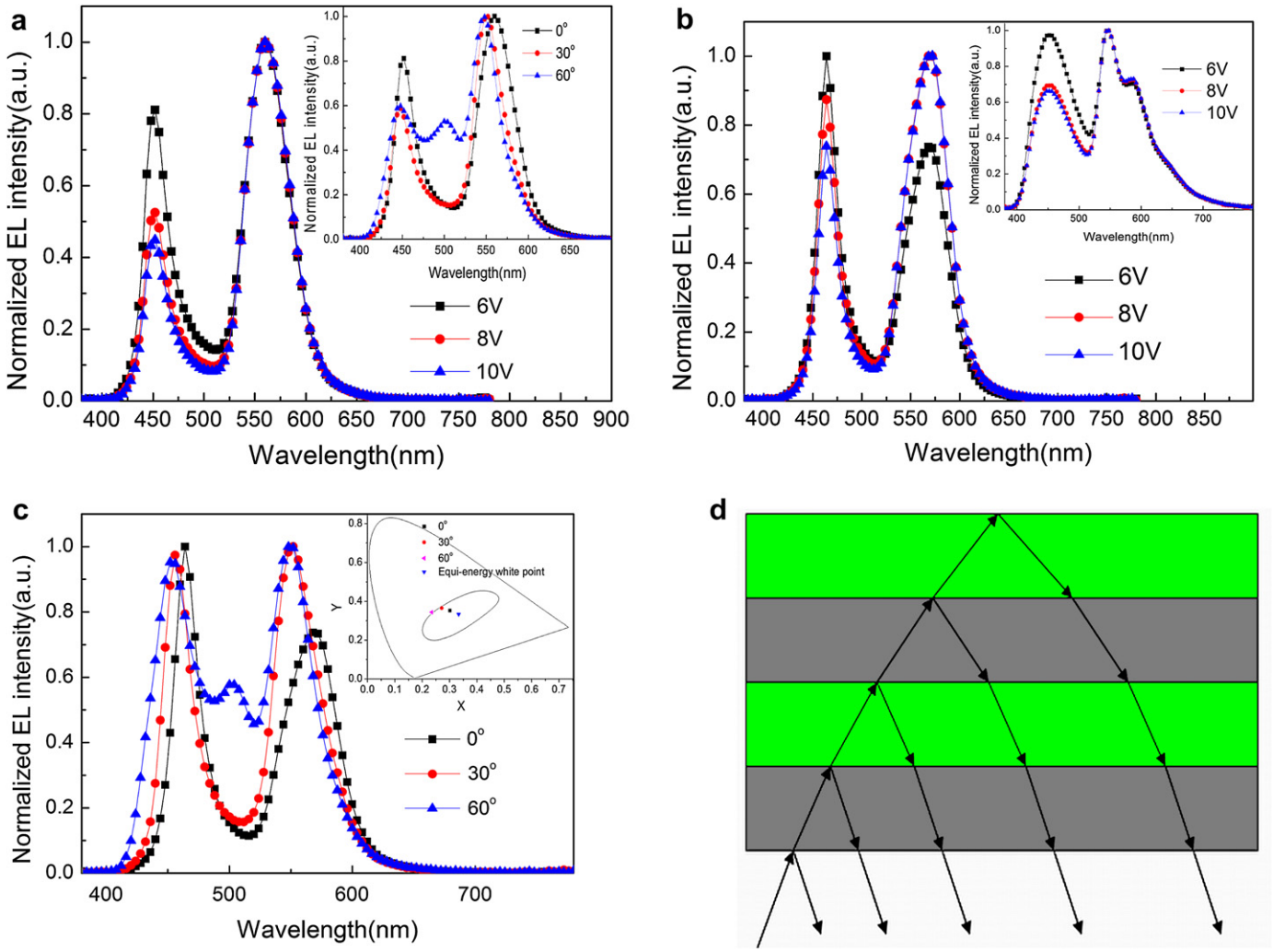

Fig. 2. (a) The normalized measured EL spectra at different voltage for device A. Insert is the normalized measured EL spectra at different viewing angle and voltage of 6 V; (b) The normalized measured EL spectra at different voltage for device B. Insert is the normalized measured EL spectra at different voltage for device C, and (c) The normalized measured EL spectra of devices B at different viewing angle and voltage of 6 V. Insert is the CIE coordinate of device B at different view angles and voltage of 6 V. (d) The structure of cathode and multiple-beam interference.

shows two peaks due to microcavity effects. As can be seen, the peak wavelength shifts to a shorter wavelength due to the microcavity effects in the TEOLEDs with increasing viewing angle. Insert is the CIE coordinates at different viewing angles and a voltage of 6 V. A white emission was obtained, and the CIE coordinates were (0.301, 0.352) at a viewing angle of 0° and changed to (0.271, 0.365) at 30° and (0.234, 0.344) at 60°. The results indicate that a better white emission can be achieved only by changing the thickness of Alq_3, but with a little decrease in current efficiency. Fig. 2(d) shows the structure and multiple-beam interference of cathode. Owing to the large difference between the refractive indices of metal and that of Alq_3, multiple-beam interference would occur within the multilayer, and a strongly wavelength-dependent phase shift and the optical properties (transmittance and reflectance) could be induced by only changing the thickness of Alq_3.

In Ref. [10], Al_2O_3 and Al_2O_3/ZrO_2 were used as the encapsulation thin-film, and the results demonstrated that Al_2O_3/ZrO_2 was more reliable than Al_2O_3 for encapsulation of devices. In our devices, the structure of cathode is Ag (20 nm)/Alq_3(x nm)/Ag(20 nm)/Alq_3(x nm) (x = 75 and 85 for device A and B, respectively). Indeed, only the first Ag layer was used as electric contact. The other layers, Alq_3(x nm)/Ag(20 nm)/Alq_3(x nm), can work as buffer layer when

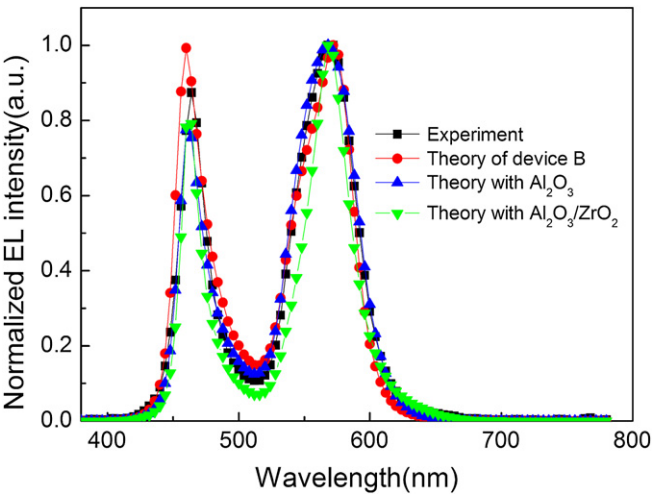

Fig. 3. The normalized measured and simulated EL spectra of the white TEOLED.

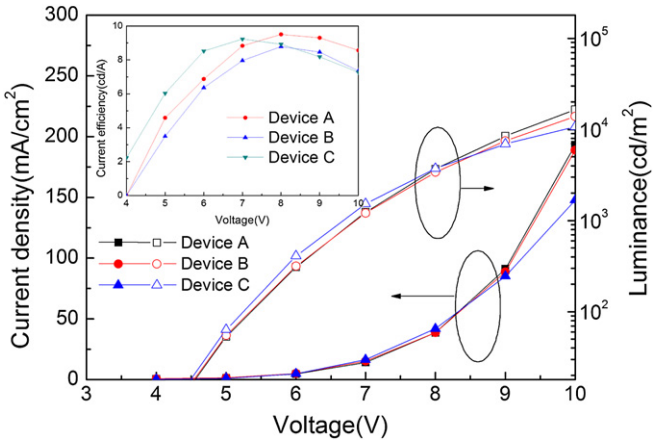

Fig. 4. The voltage-current density-luminance characteristics of the device. Insert the efficiency-voltage characteristics of the white devices.

depositing Al_2O_3 by RF magnetron sputtering. Here, we used 150 nm Al_2O_3 and Al_2O_3/ZrO_2 as the encapsulation thin-film and calculated the spectrum of device B. The theoretic spectrum of device B without encapsulation was also calculated. The results were plotted in Fig. 3. As can be seen, the simulated spectrum is in excellent agreement with experiment result. The slight difference is due to the measure error of the thickness of organic and metal layers. We can also see that the introduction of encapsulation thin-film Al_2O_3 or Al_2O_3/ZrO_2 almost do not change the emission spectrum of devices, which makes the device have almost the same CIE color coordinates as without encapsulating. The CIE coordinates are (0.334, 0.400) for device B, (0.338, 0.420) for device with Al_2O_3 encapsulating and (0.342, 0.397) with Al_2O_3/ZrO_2 encapsulating. All the results indicated that thus devices with this kind of cathode can be encapsulated directly without buffer layer.

Fig. 4 shows the voltage-current density-luminance characteristics of the devices A, B, and C. The luminance of the devices A, B and C are 16,540, 13,910, and 10,740 cd/m^2 at 10 V, respectively. Insert shows the efficiencies versus voltage characteristics of the devices. The maximum current efficiency of the devices are 9.51, 8.79, and 9.23 cd/A for devices A, B, and C, respectively. Currently, P. Freitag et al. [14] reported a high efficient metal–metal microcavity white TEOLED using pin structure. The efficiency of our device can be improved by optimizing the thickness of the emitting layers and using pin structure.

4. Conclusion

In summary, the top-emitting white organic light-emitting devices with a $(Ag/Alq_3)_2$ cathode are demonstrated. The characteristic of light emission of TEWOLEDs can be adjusted by only changing the thickness of Alq_3 layer in multi-layer cathode. The multi-layer cathode has two effects. One is to adjust the optical characteristic of the devices to achieve white emission. The other is to work as buffer layer to protect the devices when encapsulating. The results will provide guidance in fabrication of TEWOLEDs with optimum performance, such as efficiency and simplifying the process of fabrication of devices.

Acknowledgments

This work was supported by the National Natural Science Foundation of China (Grant Nos. 60937001, 60707016, 60723002, 10974071, 10774060), the Ministry of Science and Technology of China (Grant No. 2010CB327701).

References

[1] G. Gustafsson, Y. Cao, G.M. Treacy, F. Klavetter, N. Colaneri, A.J. Heeger, Nature 357 (1992) 477.
[2] G. Gu, P.E. Burrows, S. Venkatesh, S.R. Forrest, M.E. Thompson, Opt. Lett. 22 (1997) 172.
[3] A.B. Chwang, M.A. Rothman, S.Y. Mao, R.H. Hewitt, M.S. Weaver, J.A. Silvernail, K. Rajan, M. Hack, J.J. Brown, X. Chu, L. Moro, T. Krajewski, N. Rutherford, Appl. Phys. Lett 83 (2003) 413.
[4] J.S. Lewis, M.S. Weaver, IEEE J. Quantum Electron 10 (2004) 45.
[5] S.M. Chung, C.S. Hwang, J.I. Lee, S.H. Park, Y.S. Yang, L.M. Do, H.Y. Chu, Synth. Met. 158 (2008) 561.
[6] F.L. Wong, M.K. Fung, S.L. Tao, S.L. Lai, W.M. Tsang, K.H. Kong, W.M. Choy, C.S. Lee, S.T. Lee, J. Appl. Phys. 104 (2008) 014509.
[7] J. Granstrom, J.S. Swensen, J.S. Moon, G. Rowell, J. Yuen, A.J. Heeger, Appl. Phys. Lett. 93 (2008) 193304.
[8] H.K. Kim, M.S. Kim, J.W. Kang, J.J. Kim, M.S. Yi, Appl. Phys. Lett. 90 (2007) 13502.
[9] Y.G. Lee, Y.H. Choi, L.S. Kee, H.S. Shim, Y.W. Jin, S.Y. Lee, K.H. Koh, S. Lee, Org. Electron. 10 (2009) 1352.
[10] J. Meyer, D. Schneidenbach, T. Winkler, S. Hamwi, T. Weimann, P. Hinze, S. Ammermann, H.H. Johannes, T. Riedl, W. Kowalsky, Appl. Phys. Lett. 94 (2009) 233305.
[11] H. Kanno, Y.R. Sun, S.R. Forrest, Appl. Phys. Lett. 86 (2005) 263502.
[12] S.F. Hsu, C.C. Lee, S.W. Hwang, C.H. Chen, Appl. Phys. Lett. 86 (2005) 253508.
[13] M.T. Lee, M.R. Tseng, Curr. Appl. Phys. 8 (2008) 616.
[14] P. Freitag, S. Reineke, S. Olthof, M. Furno, B. Lüssem, K. Leo, Org. Electron. 11 (2010) 1676.
[15] M.S. Kim, C.H. Jeong, J.T. Lim, G.Y. Yeom, Thin Solid Films 516 (2008) 3590.
[16] M. Thomschke, R. Nitsche, M. Furno, K. Leo, Appl. Phys. Lett. 94 (2009) 083303.
[17] W.Y. Ji, L.T. Zhang, R.X. Gao, L.M. Zhang, W.F. Xie, H.Z. Zhang, B. Li, Opt. Express 16 (2008) 15489.
[18] Y.J. Lu, C.H. Chang, C.L. Lin, C.C. Wu, H.L. Hsu, L.J. Chen, Y.T. Lin, R. Nishikawa, Appl. Phys. Lett. 92 (2008) 123303.
[19] W.Y. Ji, L.T. Zhang, T.Y. Zhang, G.Q. Liu, W.F. Xie, S.Y. Liu, H.Z. Zhang, L.Y. Zhang, B. Li, Opt. Lett. 34 (2009) 2703.
[20] W.Y. Ji, L.T. Zhang, T.Y. Zhang, W.F. Xie, H.Z. Zhang, Org. Electron 11 (2010) 202.
[21] A.B. Djurišić, A.D. Rakić, Appl. Opt. 41 (2002) 7650.
[22] C.L. Lin, H.C. Chang, K.C. Tien, C.C. Wu, Appl. Phys. Lett. 90 (2007) 071111.
[23] C.L. Mitsas, D.I. Siapkas, Appl. Opt. 34 (1995) 1678.